

Structure of Free *Thermus flavus* 5 S rRNA at 1.3 nm Resolution from Synchrotron X-ray Solution Scattering*

Received for publication, June 8, 2000, and in revised form, July 13, 2000
Published, JBC Papers in Press, July 13, 2000, DOI 10.1074/jbc.M004974200

Sergio S. Funari[‡], Gert Rapp[‡], Markus Perbandt[‡], Karsten Dierks[§], Marco Vallazza[¶],
Christian Betzel^{||}, Volker A. Erdmann[¶], and Dmitri I. Svergun^{||**‡‡}

From the [‡]Institute of Physiological Chemistry, University Hospital Hamburg, c/o Deutsches Elektronen Synchrotron, Building 22a, Notkestraße 85, 22603 Hamburg, Germany, the [§]Dierks and Partner Systemtechnologie, Pinneberger Weg 22–24, 20257 Hamburg, Germany, the [¶]Institute of Biochemistry, Freie Universität Berlin, Thielallee 63, 14195 Berlin, Germany, the ^{**}European Molecular Biology Laboratory, Hamburg Outstation, c/o Deutsches Elektronen Synchrotron, Notkestraße 85, 22603 Hamburg, Germany, and the ^{‡‡}Institute of Crystallography, Russian Academy of Sciences, Leninsky prospect 59, 117333 Moscow, Russia

The shape of free *Thermus flavus* 5 S rRNA in solution at 1.3 nm resolution is restored from synchrotron x-ray scattering data using an *ab initio* simulated annealing algorithm. The free 5 S rRNA is a bent elongated molecule displaying a compact central region and two projecting arms, similar to those of the tRNA. The atomic models of the 5 S rRNA domains A-D-E and B-C in the form of elongated helices can be well accommodated within the shape, yielding a tentative model of the structure of the free 5 S rRNA in solution. Its comparison with the recent protein-RNA map in the ribosome (Svergun, D. I., and Nierhaus, K. H. (2000) *J. Biol. Chem.* 275, 14432–14439) indicates that the 5 S rRNA becomes essentially more compact upon complex formation with specific ribosomal proteins. A conceivable conformational change involves rotation of the B-C domain toward the A-D-E domain. The model of free 5 S rRNA displays no interactions between domains E and C, but such interactions are possible in the bound molecule.

Ribosomal 5 S rRNA, an essential component of the ribosome, is approximately 120 nucleotides long. The ribosomal particles lacking the 5 S rRNA have a strongly reduced activity in protein synthesis (1–3), in particular, reduced peptidyl transferase activity. Because of its functional importance and the fact that the 5 S rRNA interacts specifically with several ribosomal proteins (4), it is of great interest to know the three-dimensional structure or a reliable shape of this RNA molecule. Nearly 1000 different prokaryotic and eukaryotic 5 S rRNA sequences have been determined so far. The predicted secondary structure (5) is shown in Fig. 1. The size of the 5 S rRNA limits the possibility of its three-dimensional structure determination by nuclear magnetic resonance (NMR). Therefore, in the past, we tried to crystallize several 5 S rRNA species (6, 7). The crystals of an isolated 5 S rRNA suitable for the x-ray analysis were obtained particularly from the thermophilic bac-

terium *Thermus flavus*. These crystals, however, diffract only to about 0.75 nm resolution and are extremely sensitive to radiation, even under cryogenic conditions. The intrinsic flexibility of the whole 5 S rRNA molecule and small differences in the primary structure seem to influence significantly the quality of the crystals. The *T. flavus* 5 S rRNA was then divided into five domains, A through E, and these domains were chemically synthesized and crystallized for x-ray analysis (8, 9). In parallel, we began to analyze the shape of the entire 5 S rRNA in solution using small angle scattering, an established method of monitoring the low resolution structure of biological macromolecules (10). Recently, new approaches have been developed to *ab initio* restore low resolution structure from the scattering data (11, 12), and these were successfully applied to study proteins and ribosomes (13–15). In the present paper, an *ab initio* low resolution model of the free 5 S rRNA in solution is derived from synchrotron radiation small angle x-ray scattering (SAXS)¹ data. The atomic models of the 5 S rRNA fragments are tentatively positioned inside the low resolution shape. The model obtained may be further used for crystallographic molecular replacement studies, as well as for the analysis of the complex formation with binding proteins in solution.

EXPERIMENTAL PROCEDURES

Isolation and Purification—The *Escherichia coli* cells from strain MRE600 were grown at 37 °C in a Luria broth medium. The 70 S ribosomes were isolated by previously described extraction and centrifugation steps (2). The intact ribosomes were dissociated into their 30 and 50 S subunits at magnesium concentrations below 5 mM (1). The 5 S rRNA was separated from the large ribosomal subunit by saccharose gradient, phenol extraction and subsequently purified by Sephadex G150 gel chromatography as well as hydrophobic affinity interaction chromatography. In addition *T. flavus* 5 S rRNA was produced by *in vitro* transcription. Because of large yields of up to 5 mg/ml, sufficient RNA material can be generated at low cost and within a short time compared with the conventional isolation procedure. The reconstitution of ribosomal proteins from *Bacillus stearothermophilus* with 5 S rRNA of different species resulted in functionally intact 50 S subunits active in polypeptide synthesis (3). This finding emphasizes that the three-dimensional structure of the ribosomal 5 S rRNA is highly conserved, making it possible to replace the 5 S rRNA from *E. coli* by that from *T. flavus*. Two synthetic DNA oligonucleotides coding for the 5' and 3' regions of *T. flavus* 5 S rRNA with an overlapping area of 25 bases were annealed by stepwise cooling from 70 to 54 °C within 17 min. A double-stranded template was generated by elongation with *Pfu* polymerase for 10 min. Restriction sites and T7 promoter were introduced by primers used in the following polymerase chain reaction. The product was blunt end-ligated into the vector pUC18 (2686 base pair) and transformed

* This research was supported by the European Union Biotechnology Program (Grant BIO4-CT97-2143 to D. I. S.) and by the Bundesministerium für Bildung und Forschung via the network of RNA Technology (RiNA) GmbH, the Deutsche Forschungsgemeinschaft (SFB 344-D6). The costs of publication of this article were defrayed in part by the payment of page charges. This article must therefore be hereby marked "advertisement" in accordance with 18 U.S.C. Section 1734 solely to indicate this fact.

|| To whom correspondence should be addressed. Tel.: 49 40 89902-125; Fax: 49 40 89982-149; E-mail: svergun@embl-hamburg.de; or Tel.: 49 40 8998-4744; Fax: 49 40 8998-4747; E-mail: betzel@unisig1.desy.de.

¹ The abbreviations used are: SAXS, small angle x-ray scattering; DAM, dummy atoms model.

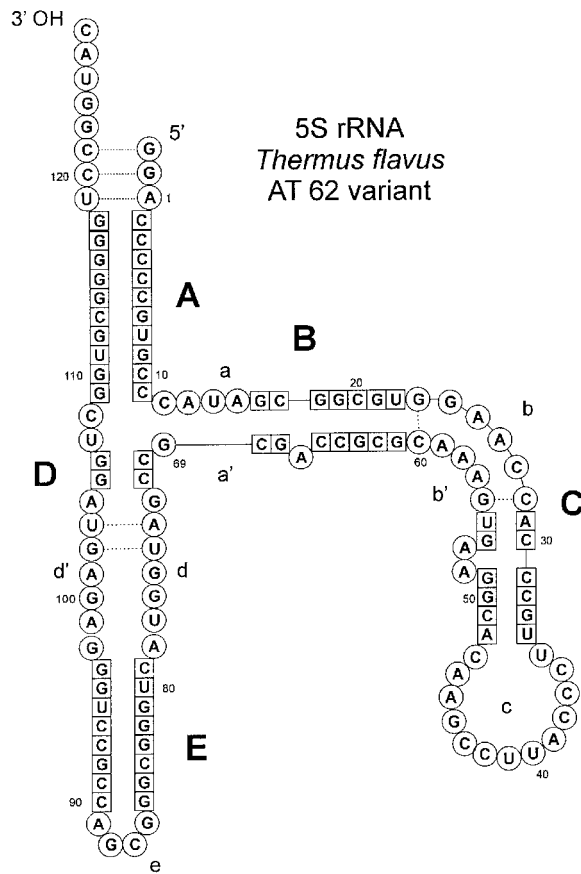


FIG. 1. Secondary structure of the *T. flavus* 5 S rRNA according to biochemical and analytical methods such as enzymatic cleavage, chemical modification, and sequence alignment studies (5).

into *E. coli* JM109 cells sensitive to blue/white screening. The correct sequence of the insert was checked by sequencing the isolated plasmids from several clones. After plasmid linearization with *EcoRV* (NEB), the wild-type 5 S rRNA of *T. flavus* was synthesized during run off transcription in the RiboMAX system (Promega). The RNA was purified by phenol extraction and gel filtration. The samples were concentrated by ethanol precipitation and resuspended in 5 mM $MgCl_2$ buffer. Purity and homogeneity of the product were analyzed by UV spectroscopy, denaturing urea polyacrylamide gel electrophoresis (6), and dynamic light scattering. Monodispersity of the samples was controlled by dynamic light scattering using a newly developed experimental set-up (16).

Scattering Experiments and Data Processing—The SAXS data were collected using standard procedures on the X33 camera (17–19) of EMBL at the storage ring DORIS III of the Deutsches Elektronen Synchrotron (DESY) and multiwire proportional chambers with a delay line readout (20). The scattering curves at the solute concentrations 0.5, 1, 2, 3, 5, 7, and 10 mg/ml were measured at sample detector distances of 3.5 and 1.4 m, covering the momentum transfer ranges $0.25 < s < 1.8 \text{ nm}^{-1}$ and $0.40 < s < 5.5 \text{ nm}^{-1}$, respectively ($s = 4\pi \sin\theta/\lambda$, where 2θ is the scattering angle and $\lambda = 0.15 \text{ nm}$ is the x-ray wavelength). The data were normalized to the intensity of the incident beam corrected for the detector response, the scattering of the buffer was subtracted, and the difference curves were scaled for concentration using the program SAPOKO.² The reduced data sets at low angles were extrapolated to zero concentration following standard procedures (10). The final composite scattering curve was obtained by merging the extrapolated low angle data with the curve recorded at higher angles at 10 mg/ml. The maximum dimension D_{\max} of the 5 S rRNA was estimated from the experimental data using the orthogonal expansion program ORTOGNOM (21). The radii of gyration R_g at different concentrations were evaluated using the Guinier approximation (10) and the indirect Fourier transform program GNOM (22, 23). The latter program was also

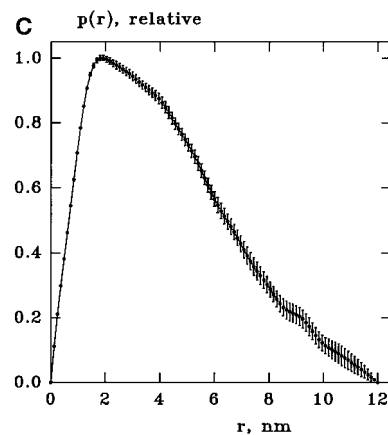
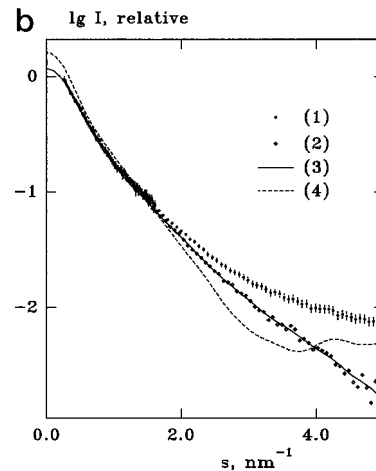
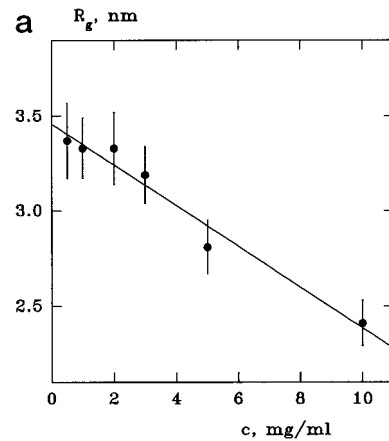


FIG. 2. *a*, concentration dependence of the radius of gyration computed from the scattering by the 5 S rRNA solutions. *b*, x-ray scattering from the 5 S rRNA in solution and scattering calculated from the models. 1, composite experimental curve; 2, shape scattering curve after subtraction of a constant; 3, scattering from the *ab initio* dummy atom model; 4, scattering from the model of Westhof *et al.* (26). *c*, distance distribution function of the 5 S rRNA evaluated by the program GNOM.

used to compute the distance distribution function $p(r)$. Prior to the shape analysis, a constant was subtracted from the experimental data to ensure that the intensity at higher angles decays as s^{-4} following Porod's law (24) for homogeneous particles. The value of this constant is determined automatically by the shape determination program DAMMIN (described under "Shape Determination") from the outer part of the curve by drawing a straight line in coordinates $s^4 I(s)$ versus s^4 . This procedure reduces the contribution from scattering due to the internal particle structure and yields an approximation of the "shape scattering" curve (*i.e.* scattering from the excluded volume of the particle filled by constant density). The Porod volume V_p (24) was calculated from the shape scattering curve as described (10).

² D. I. Svergun and M. H. J. Koch, unpublished results.

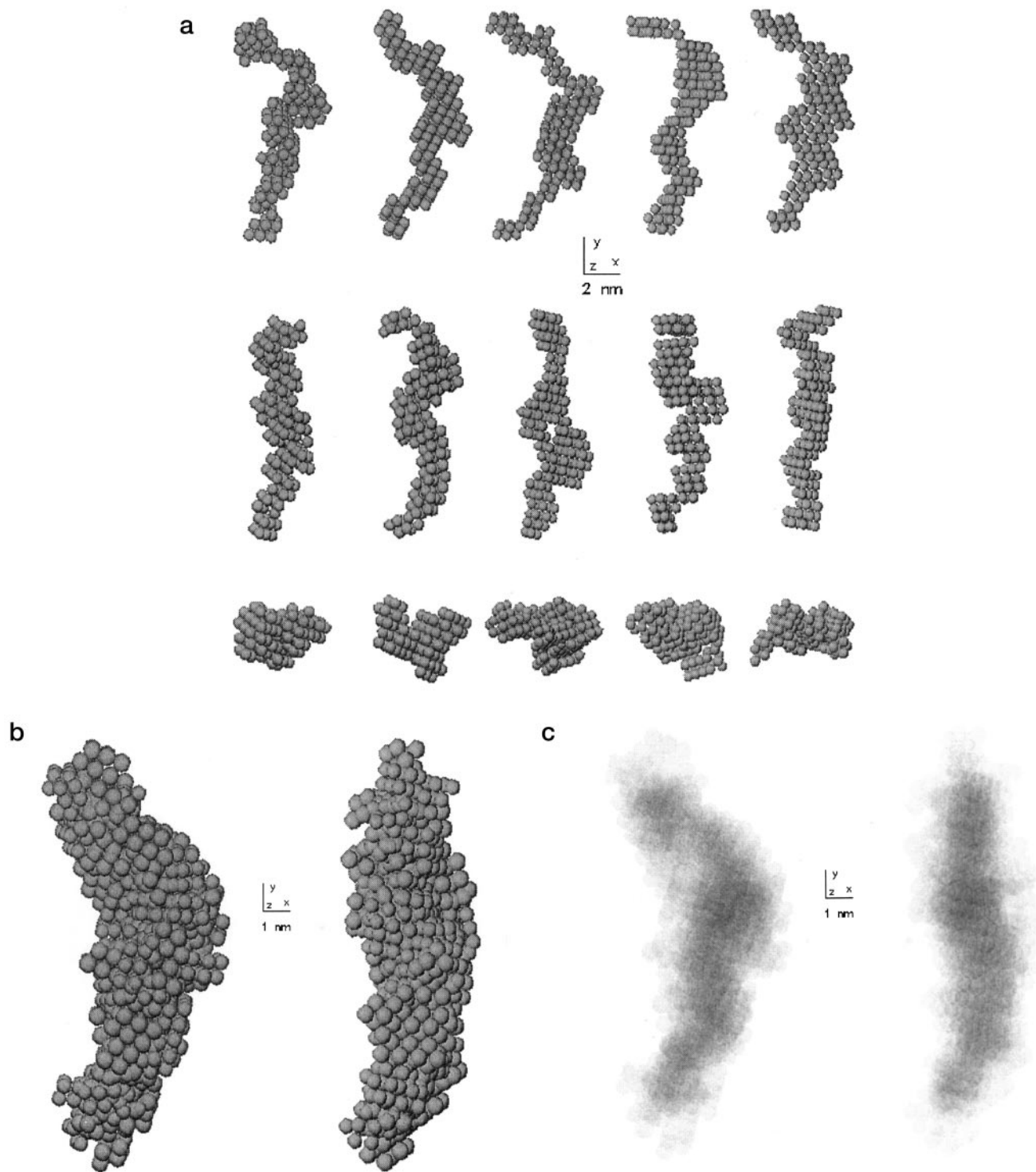


FIG. 3. *a*, low resolution models of the 5 S rRNA obtained *ab initio* in five independent shape determination runs (from left to right). The middle and bottom rows are rotated counterclockwise by 90° around the y and x axes, respectively. *b* and *c*, superposition of 10 low resolution models of the 5 S rRNA displayed as solid and semitransparent spheres, respectively.

Shape Determination—The shape of the 5 S rRNA was restored from the experimental data using an *ab initio* method (12). A sphere of diameter D_{\max} is filled by a regular grid of points corresponding to a dense hexagonal packing of small spheres (dummy atoms) of radius $r_0 \ll D_{\max}$. The structure of the dummy atoms model (DAM) is defined by a configuration vector X assigning an index to each atom (0 corresponds to solvent and 1 to the solute particle). The scattering intensity $I(s)$ from the DAM is evaluated as

$$I(s) = 2\pi^2 \sum_{l=0}^{\infty} \sum_{m=-l}^l |A_{lm}(s)|^2, \quad (\text{Eq. 1})$$

where the partial amplitudes $A_{lm}(s)$ are as follows.

$$A_{lm}(s) = i^l \sqrt{2/\pi} v_a \sum_j j_l(sr_j) Y_{lm}^*(\omega_j) \quad (\text{Eq. 2})$$

Here, the sum runs over the dummy atoms with $X_j = 1$ (particle atoms), r_j , ω_j are their polar coordinates, $v_a = (4\pi r_0^3/3)/0.74$ is the displaced volume per dummy atom, $j_l(x)$ and $Y_{lm}(\omega)$ denote the spherical Bessel function and the spherical harmonics, respectively. In keeping with the low resolution of the solution scattering data, the method searches for a compact interconnected configuration X , minimizing the discrepancy

χ between the calculated and the experimental curves,

$$\chi = \sqrt{\frac{1}{N-1} \sum_{j=1}^N \left[\frac{I(s_j) - I_{\text{exp}}(s_j)}{\sigma(s_j)} \right]^2} \quad (\text{Eq. 3})$$

where N is the number of the experimental points and $I_{\text{exp}}(s_k)$ and $\sigma(s_k)$ are the experimental intensity after a constant subtraction and its standard deviation in the k -th point, respectively. Starting from a random configuration, simulated annealing (25) is employed for the minimization. The details of the program DAMMIN are described elsewhere (Refs. 12, 14, and 15; see also the EMBL Web page).

Atomic Models—The atomic coordinates of the theoretical model of the 5 S rRNA from *Xenopus laevis* (26) were taken from the Protein Data Bank (27), entry code 1rrn. The solution scattering curve from this model was computed using a modified version of the program CRY SOL (28). The atomic models of the 5 S rRNA fragments A, D, and E, available from x-ray crystallography (Refs. 29–31; entry codes 364D, 361D, and 353D, respectively), were used as templates to fit into the low resolution shape. The models of the 5 S rRNA were displayed on a SUN SPARC-20ZX work station using the program ASSA (32) and on a SGI O₂ work station using the program O (33).

RESULTS

The apparent radius of gyration of the 5 S RNA in solution decreases with concentration (Fig. 2a), which is typical for solutions with repulsive interactions. The value $R_g = 3.46 \pm 0.05$ nm is obtained after extrapolation to infinite dilution. The composite SAXS curve from the 5 S rRNA extrapolated to zero concentration is presented in Fig. 2b. The maximum dimension and the radius of gyration of the particle are 12.0 ± 0.5 and 3.44 ± 0.05 nm, respectively, in good agreement with the values reported in earlier solution scattering studies (34, 35). The distance distribution function $p(r)$ in Fig. 2c is typical for an elongated particle. The shape scattering curve after a constant subtraction (Fig. 2b, curve 2) yields the Porod volume of 37 ± 2 nm³. This volume corresponds well to the dry volume of the 5 S RNA (38.8 nm³) computed from its molecular mass, assuming the partial specific volume of 0.53 cm³/g (36). The above results confirm that the solutions of the 5 S rRNA are monodisperse and that the shape scattering curve can be used for the shape analysis.

Ten independent *ab initio* shape determinations were performed starting from different random configurations within a spherical search volume with the diameter $D_{\text{max}} = 12$ nm. Different packing radii of the dummy atoms were used ($r_0 = 0.4, 0.35,$ and 0.32 nm, corresponding to the numbers of dummy atoms $M = 2550, 3660,$ and 4897 , respectively). The independently restored models had the radius of gyration of 3.49 ± 0.05 nm, volume 36.7 ± 1.0 nm³ and the maximum dimension 11.7 ± 0.3 nm; they all provided nearly identical fits to the data illustrated in Fig. 2b (curve 3) with the discrepancy $\chi = 0.42$. As the method yields models at an arbitrary orientation and handedness, the models were appropriately rotated and shifted for comparison. The overall appearance of the models displayed in Fig. 3a for five restorations was very similar; all of them were bent elongated particles with a cross-section diameter of about 2 nm as expected for an RNA strand. However, differences were observed in finer structural details. Given that the independently restored models yield nearly identical scattering patterns, the ambiguity illustrated in Fig. 3a had to be attributed to the low resolution of the scattering data.

Analysis of the results of independent restorations permits one to further refine the solution and to build the most probable model of the 5 S rRNA. For this process, all of the restored configurations rotated to best match each other were remapped onto a grid of densely packed spheres with $r_0 = 0.3$ nm. It is conceivable that the overlap of the 10 models in Fig. 3b encloses the actual shape of the 5 S rRNA in solution. Already a visual inspection of this overlap displayed as semitransparent spheres in Fig. 3c reveals the most probable shape of the

particle as a darker core formed by the dummy atoms with highest repetition rates. To build the final model, the shape determination was performed using the overlap in Fig. 3b ($M = 705$ dummy atoms) as a search volume instead of the spherical one. The shape of the 5 S rRNA thus obtained (Fig. 4a) is very similar to the probable shape represented in Fig. 3b. Independent restorations using the overlap in Fig. 3b as the search volume yielded only minor rearrangements of several dummy atom indices on the particle border compared with the final configuration in Fig. 4a.

The appearance of the *ab initio* model is rather similar to that of the theoretically predicted structure of the 5 S rRNA from *X. laevis* by Westhof *et al.* (26) inasmuch as both models consist of two elongated arms (helices). This agreement was unexpected, as the integral parameters of the Westhof model ($R_g = 3.82$ nm, $D_{\text{max}} = 14.0$ nm) differed significantly from the experimental values, and the calculated scattering profile (Fig. 2b, curve 4) yielded a poor fit to the experimental curve with $\chi = 5.1$. Previous models of the free 5 S rRNA derived from SAXS data (34, 35) supported a Y configuration with two shorter and one longer helix. In contrast, our data indicate that the 5 S rRNA in solution consists of two longer and one shorter helix.

The obtained shape permits one to build a tentative model of the entire 5 S rRNA using the atomic models of its fragments. The structure of the separated and extended section including domains A, D, and E (Fig. 1) was available from Correll *et al.* (29), and the rest of the molecule (domains B and C) was taken from the Westhof theoretical model (26). These two fragments were interactively fitted into the low resolution model as displayed in Fig. 4a. The surface representation of the final model of the free 5 S rRNA in solution thus obtained is displayed in Fig. 4b.

DISCUSSION

According to the sampling theorem (37–38), the number of degrees of freedom associated with the scattering curve in Fig. 2a is $N_s = D_{\text{max}} s_{\text{max}}/\pi \approx 20$. As the search models nominally contain $M \approx 10^3$ parameters (indices of dummy atoms), a natural question arises whether the information content in the scattering data justifies the *ab initio* restoration. First, it should be stressed here that the DAMs in Figs. 3 and 4a are still low resolution models, despite the small radii of the dummy atoms used (from 0.3 to 0.4 nm). The resolution of a DAM, and thus that of the final model in Fig. 4a, is defined solely by the range of the data fitted ($2\pi/s_{\text{max}} \approx 1.3$ nm); this is best illustrated by the models in Fig. 3a, which provide roughly the same degree of detail despite different packing radii used. On one side, the variety of models in Fig. 3a yielding identical scattering curves in the fitting range demonstrates that the solution of the *ab initio* shape determination problem is ambiguous. On the other side, all of these models display similar gross structure and differ only in the finer details. This situation resembles, to some extent, particular problems of NMR spectroscopy, where different chain configurations yield virtually the same discrepancy with the experimental data. The refined shape in Fig. 4a may be considered an analogue of the averaged structure provided by the NMR technique. The successful alignment of the atomic models of the 5 S rRNA fragments into this shape adds further credit to the *ab initio* model.

Earlier cross-linking experiments with phenyldiglyoxal between residues 41 and 72 (39) suggested that tertiary interactions exist between domains E and C. According to our model (Fig. 4, a and b), these domains are well separated in the unbound 5 S rRNA in solution. Fig. 4c displays our model of the free 5 S rRNA along with the recent protein-RNA map of the 50 S ribosomal subunit *E. coli* obtained from x-ray and neutron

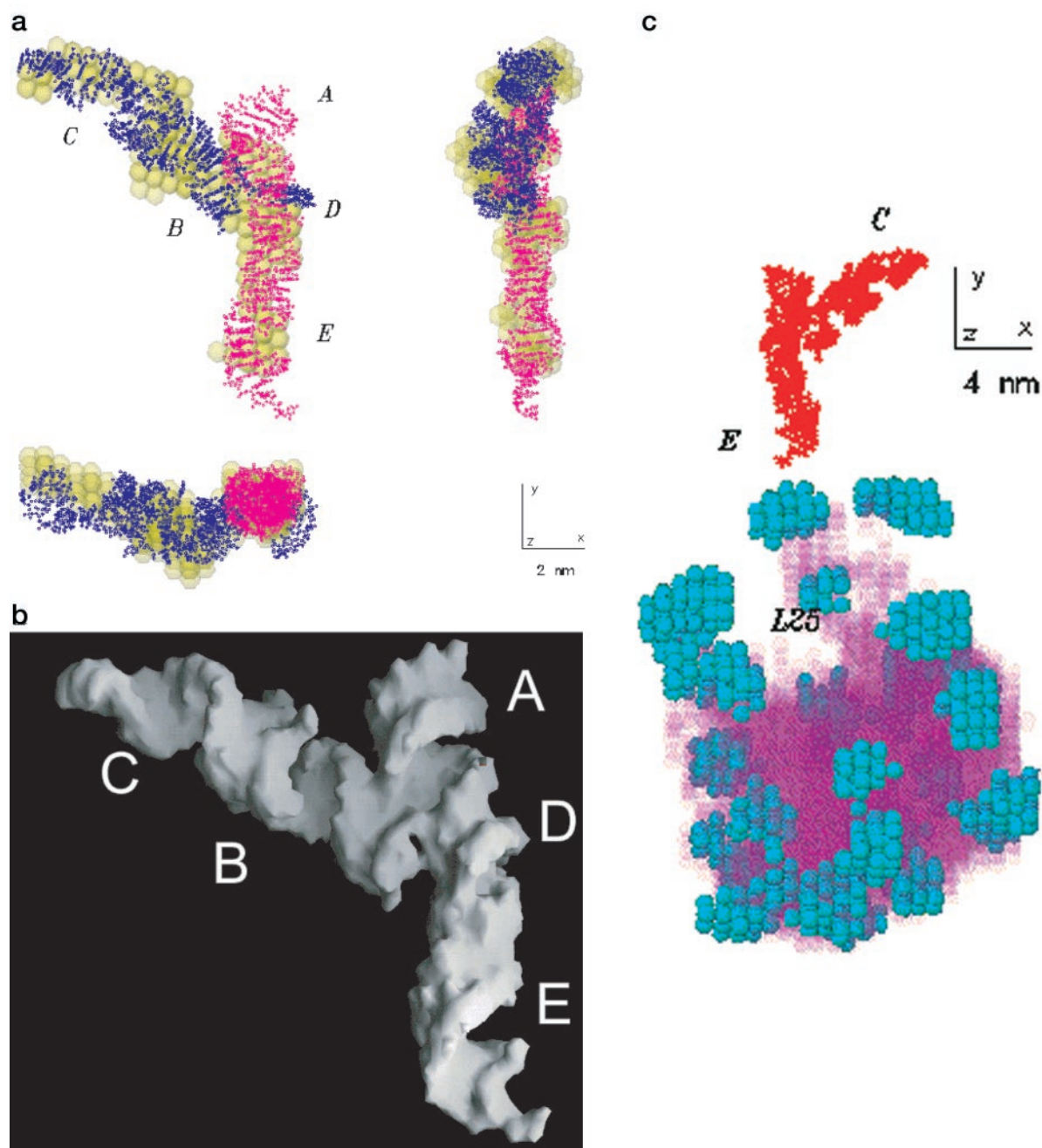


FIG. 4. *a*, the final overall shape of the 5 S rRNA (semitransparent yellow spheres) superimposed with the atomic models of the domains A-D-E (29) in blue and of a fragment containing domains B and C (26) in red. The upper left panel is displayed in the same orientation as in Fig. 3a rotated counterclockwise by 55° in the figure plane. The right and bottom panels are rotated counterclockwise by 90° around the y and x axes with respect to the upper left panel. *b*, surface presentation of the final model of 5 S rRNA. The approximate angle between the directions of the helices A-D-E and B-C is about 130° . *c*, comparison of the final model of the 5 S rRNA (red dots) with the protein-rRNA map in the 50 S ribosomal subunit *E. coli* (15). Cyan spheres indicate the volumes occupied by ribosomal proteins, and transparent magenta spheres represent the rRNA moiety. The radius of the sphere, 0.5 nm. The tentative position of the ribosomal protein L25 and the domains on the free 5 S rRNA are labeled.

scattering (15). The region of interest is at the top of the subunit, where an RNA fragment is complexed with three ribosomal proteins. This fragment is identified as a bound 5 S rRNA and the lower protein as L25 (15). The orientation of the free 5 S rRNA molecule in Fig. 4c was selected to have the domain E bound to L25 (40, 41). This comparison of the free and bound 5 S rRNA indicates that the 5 S rRNA becomes essentially more compact when forming a complex with specific ribosomal proteins. A conceivable structural rearrangement involves rotation of the domain B-C toward A-B-E (by about 60° clockwise in the plane of Fig. 4c). Such a rotation would also bring domains E and C closer together and enable the cross-

links observed in former studies (39). Yet more information on the mechanism of the complex formation would be revealed by comparison with a bound 5 S rRNA expected to be identified in the x-ray crystallographic maps of the 50 S subunit (42).

The present *ab initio* model of a free 5 S rRNA provides a basis for further crystallographic molecular replacement studies and also for the analysis of RNA-protein complexes in solution and in crystals.

REFERENCES

1. Nomura, M., and Erdmann, V. A. (1970) *Nature* **228**, 744-748
2. Erdmann, V. A., Fahnestock, S., Higo, K., and Nomura, M. (1971) *Proc. Natl. Acad. Sci. U. S. A.* **68**, 2932-2936

3. Hartmann, R. K., Vogel, D. W., Walker, R. T., and Erdmann, V. A. (1988) *Nucleic Acids Res.* **16**, 3511–3524
4. Horne, J., and Erdmann, V. A. (1972) *Mol. Gen. Genet.* **119**, 337–344
5. Specht, T., Wolters, J., and Erdmann, V. A. (1990) *Nucleic Acids Res.* **18**, (suppl.) 2215–2230
6. Lorenz, S., Betzel, C., Raderschall, E., Dauter, Z., Wilson, K. S., and Erdmann, V. A. (1991) *J. Mol. Biol.* **219**, 399–402
7. Lorenz, S., Betzel, Ch., Fuerste, J. P., Bald, R., Zhang, M., Raderschall, E., Dauter, Z., Wilson, K. S., and Erdmann, V. A. (1993) *Acta Crystallogr. Sect. D* **49**, 418–420
8. Lorenz, S., Perbandt, M., Lippmann, C., Moore, K., DeLucas, L.J., Betzel, C., and Erdmann, V.A. (2000) *Acta Crystallogr. Sect. D* **56**, 498–500
9. Nolte, A., Klußmann, S., Lorenz, S., Bald, R., Betzel, Ch., Dauter, Z., Wilson, K. S., Fuerste, J. P., and Erdmann, V. A. (1995) *FEBS Lett.* **374**, 292–294
10. Feigin, L. A., and Svergun, D. I. (1987) *Structure Analysis by Small-angle X-ray and Neutron Scattering*, Plenum Press, New York
11. Svergun, D. I., Volkov, V. V., Kozin, M. B., and Stuhrmann, H. B. (1996) *Acta Crystallogr. Sect. A* **52**, 419–426
12. Svergun, D. I. (1999) *Biophys. J.* **76**, 2879–2886
13. König, S., Svergun, D. I., Volkov, V. V., Feigin, L. A., and Koch, M. H. J. (1998) *Biochemistry* **37**, 5329–5334
14. Svergun, D. I., Malfois, M., Koch, M. H. J., Wigneshweraraj, S. R., and Buck, M. (2000) *J. Biol. Chem.* **275**, 4210–4214
15. Svergun, D. I., and Nierhaus, K. H. (2000) *J. Biol. Chem.* **275**, 14432–14439
16. Schulze, T. (1996) *Ein Echtheitssystem zur Messung der dynamischen Lichtstreuung in Flüssigkeiten*. M. Sc. thesis, University Hamburg, Hamburg, Germany
17. Koch, M. H. J., and Bordas, J. (1983) *Nucl. Instrum. Methods* **208**, 461–469
18. Boulin, C. J., Kempf, R., Koch, M. H. J., and McLaughlin, S. M. (1986) *Nucl. Instrum. Methods Sect. A* **249**, 399–407
19. Boulin, C. J., Kempf, R., Gabriel, A., and Koch, M. H. J. (1988) *Nucl. Instrum. Methods, Sect. A* **269**, 312–320
20. Gabriel, A., and Dauvergne, F. (1982) *Nucl. Instrum. Methods* **201**, 223–224
21. Svergun, D. I. (1993) *J. Appl. Crystallogr.* **26**, 258–267
22. Svergun, D. I., Semenyuk, A. V., and Feigin, L. A. (1988) *Acta Crystallogr. Sect. A* **44**, 244–250
23. Svergun, D. I. (1992) *J. Appl. Crystallogr.* **25**, 495–503
24. Porod, G. (1982) in *Small-angle X-ray Scattering* (Glatter, O., and Kratky, O., eds) pp. 17–51, Academic Press, London
25. Kirkpatrick, S., Gelatt, C. D., Jr., and Vecchi, M. P. (1983) *Science* **220**, 671–680
26. Westhof, E., Romby, P., Romaniuk, P. J., Ebel, J. P., Ehresmann, C., and Ehresmann, B. (1989) *J. Mol. Biol.* **207**, 417–431
27. Bernstein, F. C., Koetzle, T. F., Williams, G. J. B., Meyer, E. E. Jr., Brice, M. D., Rodgers, J. R., Kennard, O., Shimanouchi, T., and Tasumi, M. (1977) *J. Mol. Biol.* **112**, 535–542
28. Svergun, D. I., Barberato, C., and Koch, M. H. J. (1995) *J. Appl. Crystallogr.* **28**, 768–773
29. Correll, C. C., Freeborn, B., Moore, P. B., and Steitz, T. A. (1997) *Cell* **91**, 705–712
30. Betzel, Ch., Lorenz, S., Fuerste, J. P., Bald, R., Zhang, M., Schneider, Th. R., Wilson, K. S., and Erdmann, V. A. (1994) *FEBS Lett.* **351**, 159–164
31. Perbandt, M., Nolte, A., Lorenz, S., Bald, R., Betzel, Ch., and Erdmann, V. A. (1998) *FEBS Lett.* **429/2**, 211–215
32. Kozin, M. B., Volkov, V. V., and Svergun, D. I. (1997) *J. Appl. Crystallogr.* **30**, 811–815
33. Jones, T.A., Zou, J. Y., Cowan, S. W., and Kjeldgaard, M. (1991) *Acta Crystallogr. Sect. A* **47**, 110–119
34. Müller, J. J., Zalkova, T. N., Zirwer, D., Misselwitz, R., Gast, K., Serdyuk, I. N., Welfle, H., and Damaschun, G. (1986) *Eur. Biophys. J.* **13**, 301–307
35. Österberg, R., Sjöberg, B., and Garrett, R. (1976) *Eur. J. Biochem.* **68**, 481–487
36. Serdyuk, I. N. (1979) *Methods Enzymol.* **59**, 750–775
37. Shannon, C. E., and Weaver, W. (1949) *The Mathematical Theory of Communication*, University of Illinois Press, Urbana, IL
38. Moore, P. B. (1980) *J. Appl. Crystallogr.* **13**, 168–175
39. Hancock, J., and Wagner, R. (1982) *Nucleic Acids Res.* **10**, 1257–1269
40. Stoldt, M., Wohnert, J., Ohlenschläger, O., Gorlach, M., and Brown, L. A. (1999) *EMBO J.* **18**, 6508–6521
41. Lu, M., and Steitz, T. A. (2000) *Proc. Natl. Acad. Sci. U. S. A.* **97**, 2023–2028
42. Ban, N., Nissen, P., Hansen, J., Capel, M., Moore, P. B., and Steitz, T. A. (1999) *Nature* **400**, 841–847